# A Predictive Range Expression: Applications and Limitations

Gregory Wilson, Anne Starley, Lisa Phillipps and JR Dennison, *Member, IEEE*

*Abstract*— **An empirical model of the approximate electron range of some common materials has been extended to predict the range for many diverse types of materials. The electron range of a material is the maximum distance electrons can travel through a material, before losing all of their incident kinetic energy. The original model used the Continuous Slow Down Approximation (CSDA) and the constant loss approximation (CLA) for energy deposition in a material to develop a composite analytical formula which estimated the range from <10 eV to >10 MeV with an uncertainty of ≲20% using a single empirical fitting parameter, $N_V^{eff}$. This effective number of valence electrons, was empirically calculated for >200 materials which have tabulated range and inelastic mean free path data in the NIST ESTAR and IMFP databases. Correlations of $N_V^{eff}$ with common material properties (density, atomic number, atomic weight, and band gap) were established for this large set of materials, leading to the development of a predictive formula to accurately determine $N_V^{pre}$ for arbitrary materials. This paper discusses the accuracy and limitations of the predictive formula and presents illustrative applications to several materials of interest.**

***Index Terms*— range, inelastic mean free path, electron scattering, spacecraft charging**

## NOMENCLATURE

| | |
|---|---|
| $b$ | Stopping power proportionality constant. |
| $c$ | Speed of light *in vacuum.* |
| CSDA | Continuous Slow Down Approximation. |
| $E$ | Energy. |
| $E_m$ | Mean energy lost per collision. |
| $E_{gap}$ | Band gap energy. |
| $E_{HI}$ | Energy used for the high end to calculate n. |
| $E_{LO}$ | Energy separating high and intermediate parts of range |
| $E_{HL}$ | Energy gap between HOMO and LUMO. |
| $E_p^{eff}$ | Effective plasmon energy. |
| *ESTAR* | NIST Stopping-power and range tables for electrons. |
| $f_i$ | Number of $i$-type atoms in a material. |
| $\hbar$ | Reduced Planck's constant. |
| *HOMO* | Highest occupied molecular orbital. |
| *IMFP* | Inelastic mean free path. |
| *LUMO* | Lowest unoccupied molecular orbital. |
| $\overline{M_A}$ | Mean atomic weight. |
| $m_e$ | Electron rest mass. |
| $n$ | Stopping power exponent. |
| $n_o$ | Exponent fitting parameter for $\overline{Z_A}$ in $N_V^{pre}$. |
| $n_1$ | Slope of a linear fit of $\rho_m$ versus $\overline{Z_A}$. |
| $N_A$ | Avogadro's number. |
| $N_{offset}$ | Offset fitting parameter for $\overline{Z_A}$ in $N_V^{pre}$. |
| $N_V^{eff}$ | Empirical effective number of valence electrons. |
| $N_V^{pre}$ | Predicted effective number of valence electrons. |
| $N_o$ | Scaling fitting parameter for $\overline{Z_A}$ in $N_V^{pre}$. |
| $N_1$ | Scaling fitting parameter for $\rho_m$ in $N_V^{pre}$. |
| *NIST* | National Institute of Standards and Technology. |
| $q_e$ | Electron charge. |
| $r$ | Linear correlation coefficient. |
| $R$ | Electron range. |
| $z$ | Distance along normal into a material. |
| $\overline{Z_A}$ | Mean atomic number. |
| $\beta, \gamma, C, D$ | Coefficients used in the TPP-2M formula. |
| $\varepsilon_0$ | Permittivity of free space. |
| $\lambda_{IMFP}$ | Inelastic mean free path. |
| $\rho_m$ | Mass density. |
| $\tilde{\chi}^2_{red}$ | Reduced chi squared. |

## I. INTRODUCTION

The electron range in materials, $R$, describes the maximum distance electrons of an initial incident energy can travel through a material before they lose all of their kinetic energy and come to a rest, depositing their charge. It is also described as the mean path length from a primary electron's point of incidence to where it comes to rest. It differs from the penetration depth which is the mean projection of the range onto the direction of incidence [1]. The primary energy loss mechanism for electrons is due to inelastic collisions within the material with a mean energy loss defined as the mean excitation energy. At very low energies where only a single inelastic collision is likely to occur, the range becomes synonomous to the inelastic mean free path (IFMP).

Due to the probabilistic nature of this process, the Continuous Slow Down Approximation (CSDA) is often employed to simplify the problem. In the CSDA, the rate of energy loss, $dE/dz$ (termed the total stopping power) is assumed equal to the total stopping power at every position along the penetration path; variations in energy-loss rate with energy, $E$, or with penetration depth, $z$, are neglected and discrete energy loss for individual collisions is averaged over a mean free path. A

Research was supported by funding from the NASA James Webb Space Telescope Program through Goddard Space Flight Center, a Utah State University Undergraduate Research and Creative Opportunities grant, and a fellowship from the Utah NASA Space Grant Consortium.

Greg Wilson, Anne Starley, Lisa Montierth Phillips, and JR Dennison are with the Materials Physics Group in the Physics Department at Utah State University in Logan, UT 84322 USA (e-mail: GregdWilson@gmail.com, Anne.Starley@aggiemail.usu.edu, Montierth33@gmail.com, JR.Dennison@usu.edu).

Color versions of one or more figures in this paper are available online at http://ieeexplore.ieee.org.

Digital object identifier.

further approximation can be made which assumes a constant loss approximation (CLA), approximating *dE/dz* as a constant.

In an initial study, an approximate range expression was developed by merging well known semi-empirical models for the interaction of electrons with materials in different energy regimes by employing the CSDA and the CLA; details of this model are provided in [4]. Using these approximations, a simple, continuous, composite, analytic formula—with the single empirical free parameter, $N_V^{eff}$—was used to approximate the range ($10^{-9}$ m to $10^{-2}$ m) over an extended energy span (<10 eV to >10 MeV). Agreement of model range predictions with tabulated range data in the NIST databases was found to be within ≲20% (often much less) for more than 200 conducting, semiconducting, and insulating materials [2,3,4].

Correlations of $N_V^{eff}$ from this initial study [4] with common material properties have been established for this large initial set of materials [10,11,12]. This has led to the development of a predictive formula to accurately determine $N_V^{pre}$ for arbitrary materials based solely on mass density, mean atomic number and atomic weight from stoichiometric formula, and approximate band gap energy. This paper discusses the accuracy and limitation of the predictive formula and presents illustrative applications to several materials of interest.

## II. ORIGINAL RANGE MODEL

The previously developed range model predicts the energy-dependent range, *R(E),* as a function of incident electron energy, *E*, spanning incident energies from <10 eV to >10 MeV. The model uses a *single fitting parameter,* $N_V^{eff}$ and material parameters mass density $\rho_m$, mean atomic number $\bar{Z}$, mean atomic weight $\overline{M_A}$ weighted by atomic fraction, and band gap energy $E_{gap}$ [4]. The final result is a continuous piece-wise analytic approximation to the range, described by (1), (2), (3), and (4):

$$R\left(E;N_V^{eff}\right) = \begin{cases} \left[\frac{E}{E_m}\right]\lambda_{IMFP}(E_m)\left(\frac{1-exp[-1]}{1-exp\left[-\frac{E}{E_m}\right]}\right)^2 & ;E<E_m \\ \left[\frac{E}{E_m}\right]\lambda_{IMFP}(E)\frac{1-exp[-1]}{1-exp\left[-\frac{E}{E_m}\right]} & ;E_m\le E\le E_{LO} \\ bE^n\left(1-\left[1+\left[\frac{\bar{Z}^{0.39}E}{3N_V^{eff}m_ec^2}\right]\right]^{-2}\right) & ;E>E_{LO} \end{cases} \quad (1)$$

The inelastic mean free path, $\lambda_{IMFP}(E)$ is expressed with the TPP-2M formula [5] used in conjunction with the NIST IMFP database [3]:

$$\lambda_{IMFP}(E) = E\left[E_p^{eff}\right]^{-2}[\beta ln(\gamma E) - CE^{-1} + DE^{-2}]^{-1}. \quad (2)$$

*β, γ, C* and *D* are defined in [5] and *n* and *b* are defined in [4]; all these are defined in terms of only the material parameters $\rho_m$, $\bar{Z}$, $\overline{M_A}$, $E_{gap}$, and various physical constants [4].

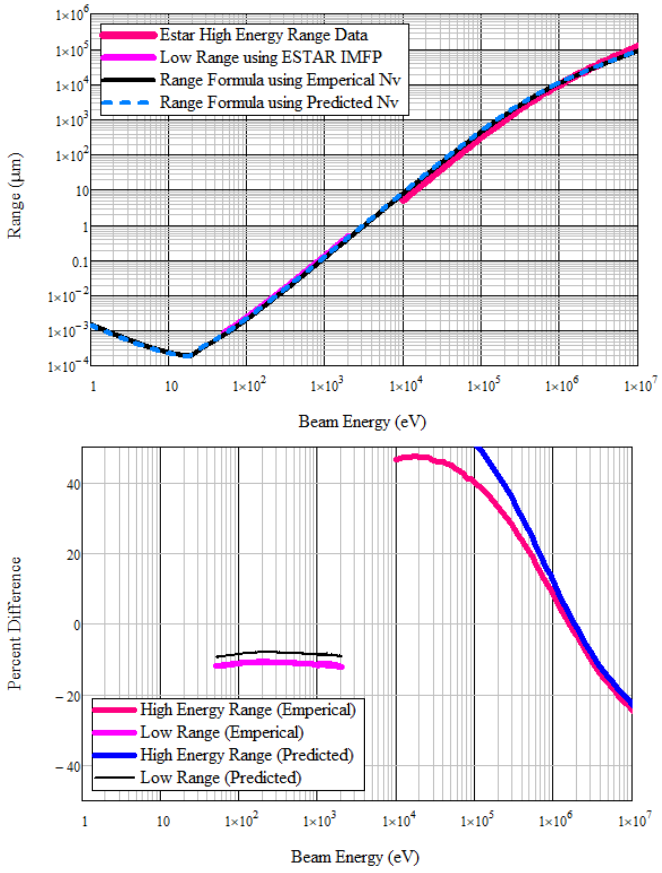


**Fig. 1. Range as a function of incident energy for Li. (a) Range calculated using both empirical and predicted $N_V^{eff}$ values as compared to NIST ESTAR range and IMFP data. (b) Percent differences for both medium and high energy regimes for Li ranges calculated for both empirical $N_V^{eff}$ and predicted $N_V^{pre}$ values, as compared to NIST ESTAR range and IMFP data.**

Here $E_m$ is equal to mean energy lost per collision occurring on average at the inelastic mean free path $\lambda_{IMFP}(E_m)$. For $E < E_m$ the range follows an approximation of the IMFP since the TPP-2M equation is not valid at these energies. As seen in Fig. 1, this curve increases for energies ≲ 50 eV due to the increase in the IMFP for low energy electrons as demonstrated in [5]; however, due to small data sets and high variabilities and uncertainties in the IMFP at low energies, these values should be considered as trends and not definitive data. In order to approximate $E_m$, the energy at which these single collisions dominate, an empirically determined factor of 2.8 [4] is multiplied by the geometric mean of the effective plasmon energy and the bandgap energy, $E_{gap}$, giving:

$$E_m = 2.8\left[\left(E_p^{eff}\right)^2 + \left(E_{gap}\right)^2\right]^{1/2}. \quad (3)$$

The effective plasmon energy, $E_p^{eff}$, for an arbitrary atomic or molecular material is defined in analogy with the bulk free-electron plasma energy for conductors—which is proportional to the square root of the number of valance electrons per atom or molecule—as

$$E_p^{eff} = \hbar\left(N_V^{eff}{q_e}^2/m_e\varepsilon_0\right)^{1/2}. \quad (4)$$

**Table I. $N_v^{eff}$ and $N_v^{pre}$ for several materials with corresponding $\tilde{\chi}^2_{red}$ values and the percent change in $N_v^{eff}$ and $N_v^{pre}$.**

| Material | $N_v^{eff}$ | $\tilde{\chi}^2_{red}(N_v^{eff})$ | $N_v^{pre}$ | $\tilde{\chi}^2_{red}(N_v^{pre})$ | % change in $N_v$ |
|---|---|---|---|---|---|
| Au | 10.814 | $5.8\cdot10^{-8}$ | 10.798 | $5.8\cdot10^{-8}$ | -0.2 |
| Si | 5.493 | $1.2\cdot10^{-7}$ | 5.607 | $2.2\cdot10^{-7}$ | 2.1 |
| Al | 5.195 | $7.4\cdot10^{-8}$ | 5.273 | $1.2\cdot10^{-7}$ | 1.5 |
| $SiO_2$ | 4.716 | $6.1\cdot10^{-8}$ | 4.472 | $5.6\cdot10^{-7}$ | -5.2 |
| $Al_2O_3$ | 4.538 | $7.0\cdot10^{-8}$ | 4.145 | $9.8\cdot10^{-7}$ | -8.7 |
| Li | 1.179 | $1.1\cdot10^{-5}$ | 1.608 | $3.2\cdot10^{-5}$ | 36.4 |

Here $q_e$ and $m_e$ are the electron charge and rest mass, $\hbar$ is the reduced Planck's constant and $\varepsilon_0$ is the permittivity of free space. Following this analogy, the free parameter $N_V^{eff}$ is termed the effective number of valence electrons per atom though it lacks direct physical meaning, as discussed in [4].

## III. Empirical Values of $N_V^{eff}$

Empirical values of $N_V^{eff}$ were derived from fits to range [2] and inelastic mean free path (IMFP) [3] values as a function of incident electron energy from two NIST databases. Tabulated values of the electron ranges at high energies using the CSDA can be found in the NIST ESTAR database spanning incident energies from ~20 keV to ~1 GeV [2]. IMFP data are found in the IMFP database spanning incident energies from ~500 eV to ~2 keV [2]. Original fits to ~20 materials [4] using (1) have now been extended to include almost all of the 249 diverse materials found in the NIST databases; the materials now fit are categorized by conduction type (74 conductors, 17 semiconductors, 74 insulators), phase (156 solids, 7 liquids, 2 gases) and composition (92 elements, 47 compounds, 21 polymers, 5 composites).

### *A. Range Accuracy*

To assess the accuracy of the range model (1), comparisons can be made several ways between the NIST database range values and range values predicted from (1) using the empirical $N_V^{eff}$ values derived from fits to the NIST databases. The agreement between range values compared in this way were found in almost all cases to give good fits, with differences typically less (often much less) than ±20% over the 50 eV<$E$<10 MeV spans.

Plots of range versus energy are shown for Al, $SiO_2$, $Al_2O_3$ and Kapton in [4], for Au in [9], and for Sr in [10]. Fig. 1(a) shows such a plot for Li, a material with one of the worst range fits (see Table 1). Fig. 1(b) shows the residual percent differences for Li between the range calculations using $N_V^{eff}$ and the NIST database values. Si, Au and Sr also have relatively very poor fits (see Table 1). As with many of the materials with relatively poorer fits, the primary disagreement for Li, Si, Au and Sr results from trying to match the higher energy ranges well above $m_ec^2$ where relativistic corrections become insufficient.

Another way to quantify the agreement between range values from the NIST databases and those predicted from (1) using $N_V^{eff}$ values is to calculate the reduced chi-squared values, $\tilde{\chi}^2_{red}$, over the full 50 eV to 10 MeV spans of NIST data. Fig. 2(a) is a plot of $\tilde{\chi}^2_{red}$ versus $N_V^{eff}$ for all the materials fitted. The mean $\tilde{\chi}^2_{red}$ is ~$6\cdot10^{-7}$, indicative of very good fits. However, the

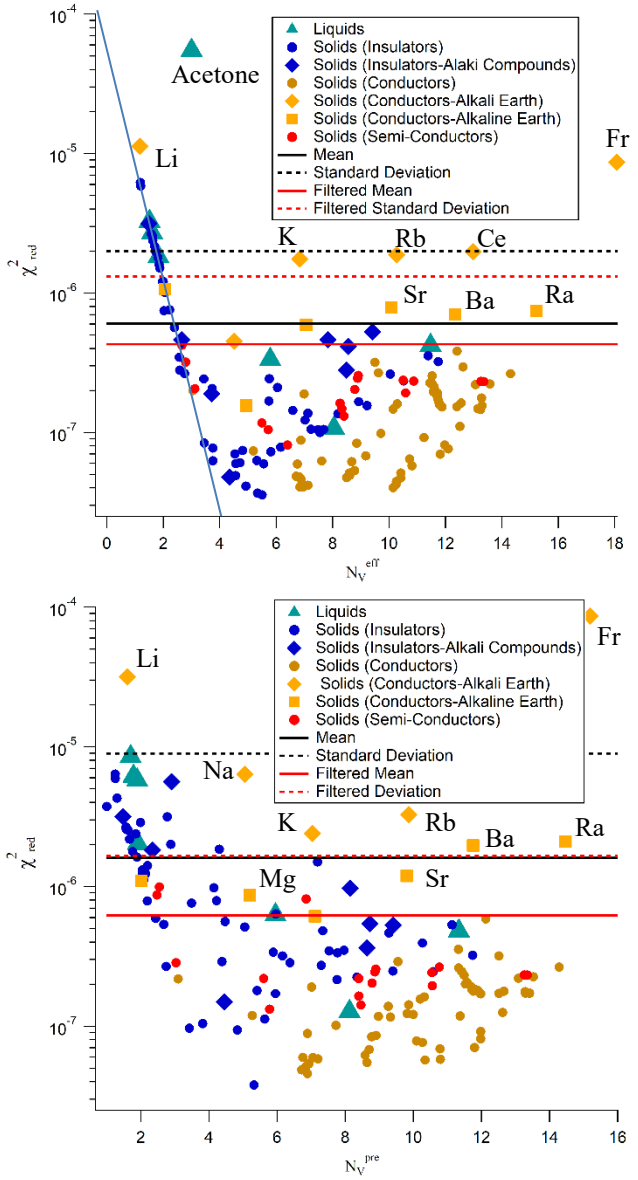


**Fig. 2. Reduced chi squared values, $\tilde{\chi}^2_{red}$, for comparisons of range values from the NIST databases to those predicted from (1) using $N_V$ values. Values for the range were calculated using: (a) the empirical values $N_V^{eff}$ determined from fits to the NIST databases and (b) the values $N_V^{pre}$ predicted using (7). Materials are categorized with symbols as noted in the legends. The mean $\tilde{\chi}^2_{red}$ (solid lines) and standard deviation of the $\tilde{\chi}^2_{red}$ values (dashed lines) for the full data set (black) and data set with alkali, alkaline and alkali halide populations removed (red) are indicated on the graphs.**

standard deviation of the $\tilde{\chi}^2_{red}$ of ~$2\cdot10^{-6}$ suggests there is a wide range of $\tilde{\chi}^2_{red}$ values.

Indeed, plotting the $\tilde{\chi}^2_{red}$ values versus $N_v$ for all of the materials revealed that the greatest errors were from a small number of materials, which were in three main populations. The first category consists of materials with $N_V^{eff} \lesssim 3$ which followed a power law trend as shown in Fig. 2(a). The second category consists of elemental alkali (Li, Na, K, Rb, Cs, Fr; yellow diamonds in Fig. 2) and alkaline earth (Be, Mg, Ca, Sr, Ba, Ra; yellow squares) metals as indicated in Fig. 2. The third category includes highly ionic alkali halide compounds (blue diamonds). When these three populations are removed, the mean $\tilde{\chi}^2_{red}$ is ~$4\cdot10^{-7}$ with a standard deviation of ~$1\cdot10^{-6}$. It is important to note, that while these three categories of materials

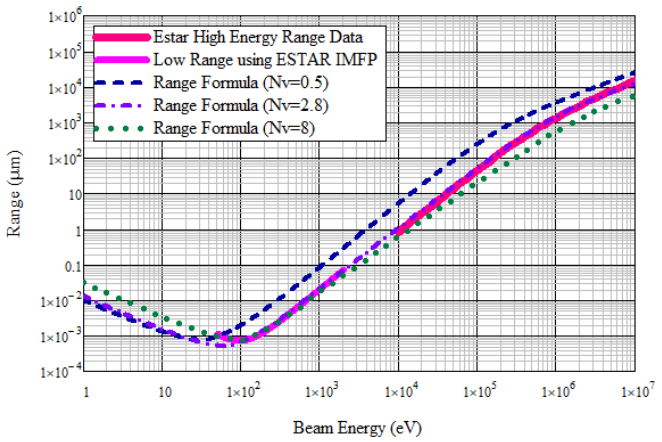


**Fig. 3. Effect of different $N_V^{eff}$ on the predicted range for $Al_2O_3$. Range fits for three different $N_V^{eff}$ values (0.10, 4.50, and 8.00) alumina are compared.**

are shown to have the greatest deviations, their $\tilde{\chi}^2_{red}$ values are still $\lesssim 1 \cdot 10^{-5}$. Even though Li has the greatest $\tilde{\chi}^2_{red}$, it still has reasonable agreement for the range when compared to NIST ESTAR range and IMFP data, with errors still $\lesssim$40% as shown in Fig 1(b).

### *B. Sensitivity to $N_V^{eff}$*

In order to estimate the effect of variances in the fitting factor $N_V^{eff}$, Fig. 3(a) shows the variations of the composite fit (1) calculated with different $N_V^{eff}$. It compares plots of range versus energy for the ceramic insulator alumina ($Al_2O_3$)—with $N_V$ set equal to 0.1, 4.5 (the calculated value from the fit), and 8.0, while other materials parameters are held constant—to the database range values. Similar comparisons for typical conductors, Al [4] and Au [9], are shown elsewhere. We find that lower values of $N_V^{eff}$ overestimate the range, while higher values of $N_V^{eff}$ underestimate the range [4]. Based on the quality of the fits to the database values, the typical uncertainty in $N_V^{eff}$ is estimated to be $\lesssim$10%. Based on these results, even with significant variance in $N_V^{eff}$, we can expect to find values that are reasonably accurate for most applications.

## IV. PREDICTIVE FORMULA FOR $N_V^{eff}$

In order to extend the usefulness of the approximate range model (1) to materials where there are no range data available to empirically find the single fitting parameter $N_V^{eff}$, a simple formula using material parameters was developed to predict $N_V^{pre}$:

$$N_V^{pre}(\overline{Z_A}) = N_o\left(\overline{Z_A}^{n_0} + N_{offset}\right). \quad (5)$$

This formula was found through extensive analysis of much more complex predictive formulas for $N_V^{pre}$ involving products of power law terms for density, mean atomic number and weight, and bandgap plus other properties including plasmon energy, conductivity, phase, and more [11, 12]. This general fit for $N_V^{pre}$ was evaluated using general least squares fit analysis methods to simultaneously determine the best estimates for fitting parameters for each material property.

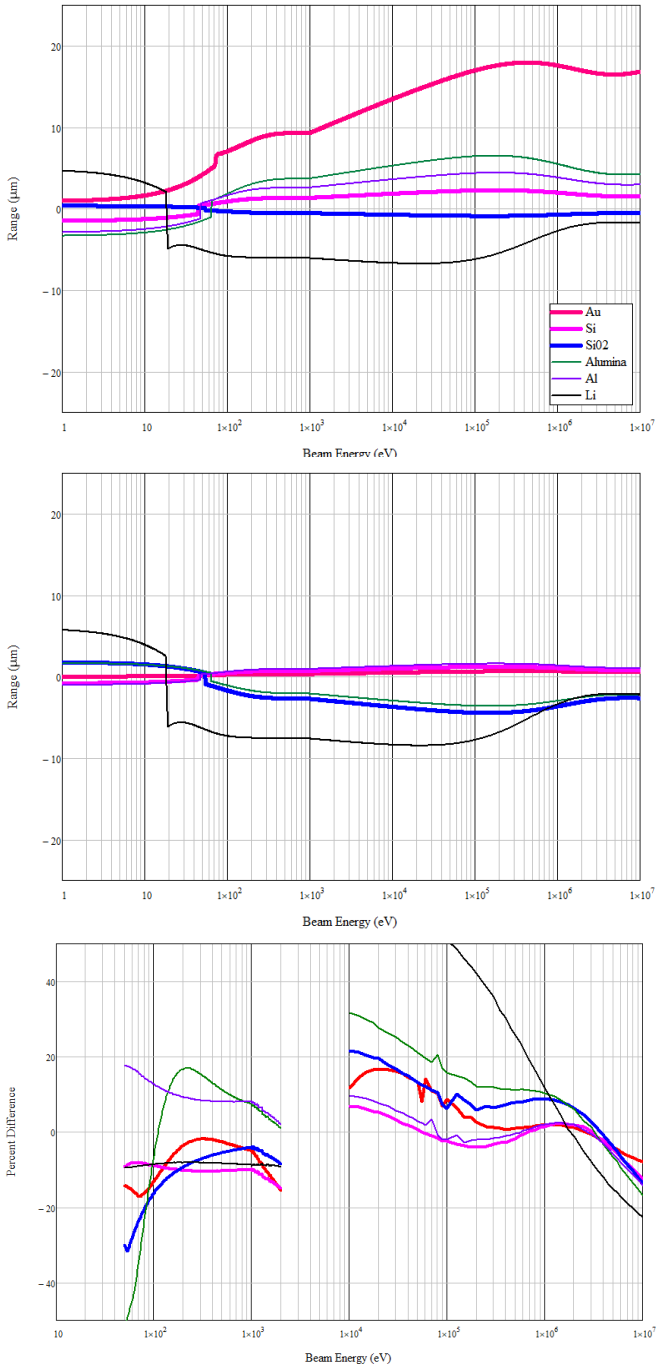


**Fig. 4. Percent difference between the calculated range using $N_V^{pre}$ and the calculated range using $N_V^{eff}$ as a function of energy, with $N_V^{pre}$ given by: (a) Eq. (5) and (b) Eq. (7). (c) Percent difference between the approximated range using $N_V^{pre}$ using Eq. (7) and the range from the NIST ESTAR range and IMFP databases. Results for Au, Si, $SiO_2$, $Al_2O_3$, Al and Li, which are particularly poor fits, are shown.**

### *A. Effect of Atomic Number Correction*

Remarkably, this predictive formula for effective number of valence electrons (5) was a function of only mean atomic number weighted by atomic fraction, $\overline{Z_A}$, which can be easily determined from the stoichiometric formula for compounds or from elemental fractions for composite materials as

$$\overline{Z_A} \equiv [\textstyle\sum_i f_i Z_{Ai}]/[\sum_i f_i] \quad (6)$$

where $f_i$ is the number of $i$-type atoms in the material and $Z_{Ai}$ is the atomic number of the $i$-type atom.

The fitting constants for (5), $N_o$, $n_o$ and $N_{offset}$, were found through least squares fits to minimize the difference between $N_V^{pre}(\overline{Z_A})$ from (5) and the empirical values for $N_V^{eff}$. Goodness of fit metrics of chi squared $\chi^2_{Nv}$ and linear correlation coefficient $r_{Nv}$ allowed quantification of the quality of these fits (see Table 2). The fitting parameters were then used to calculate values of $N_V^{pre}$ using Eq. 5.

To better assess the validity of the predictive formula (5) for $N_V^{pre}(\overline{Z_A})$, Fig. 4(a) plots the percent difference versus energy of ranges calculated with both empirical $N_V^{eff}$ and predicted $N_V^{pre}$.

### *B. Effect of Density Correction*

To assess the ability of (5) to accurately predict $N_V^{eff}$, Fig. 5(a) plots the predicted $N_V^{pre}$ values using (5) against the empirical $N_V^{eff}$ values. Lines indicate ±10% (dashed red) and ±30% (purple dot-dashed) deviations from a one-to-one linear fit (solid red), which would be expected for an exact predictive model. It is apparent that while there is strong correlation ($r = 0.984$), there is substantial scatter of ~±15% in the predictions from a perfect linear fit.

To refine (5), separate fits similar to Fig. 5(a) were made for materials subcategorized into grouping such as solids/liquids/gasses and conductors/semiconductors/insulators, with the hope that this categorization might reveal additional trends [11]. Semiconductors showed excellent agreement. Insulators showed very good agreement, with a slight downward concavity. Although conductors showed good agreement, their values oscillated about the unity line, with amplitude increasing with increasing $N_V^{eff}$. Plots in Fig. 5(b) of the residuals $(N_V^{pre} - N_V^{eff})$ [using (5)] versus empirical $N_V^{eff}$ values also exhibited these patterns.

The observed patterns were very reminiscent of the deviations from linearity seen in plots of density versus atomic number for the elements [13]. The oscillations in the density for conductors (and similar trends in atomic radius and ionization energy) are well understood in terms of how many free electrons there are in the outermost shell and specifically the electron overlap in the d and f orbitals of transition and rare earth/actinide elements due to metallic interactions between atoms.

Therefore, a simple corrective term was added to (5) dependent on the mean atomic number $\overline{Z_A}$ rather than elemental atomic number, so as to extend the correction to non-elemental materials. Using the residuals from a linear fit of $\rho_m$ versus $\overline{Z_A}$, a scaled correction factor was added to (5) giving:

$$N_V^{pre}(\overline{Z_A}, \rho_m) = N_o\left(\overline{Z_A}^{n_0} + N_{offset}\right) - N_1(\rho_m - n_1\overline{Z_A}), \quad (7)$$

where $N_1$ is a scaling factor. The parameter $n_1$ was determined solely from $\rho_m$ and $\overline{Z_A}$ values, independent of range data, as the slope of a linear fit of $\rho_m$ versus $\overline{Z_A}$; separate values were found for all materials and for materials separated by category (see Table 2). As with (5), the fitting constants for (7), $N_1$, $N_o$, $n_o$ and $N_{offset}$, were found through least squares fits to minimize the difference between $N_V^{pre}(\overline{Z_A}, \rho_m)$ from (7) and the empirical values for $N_V^{eff}$. Values for these fitting constants for all materials and for materials separated by category are listed in Table 2.

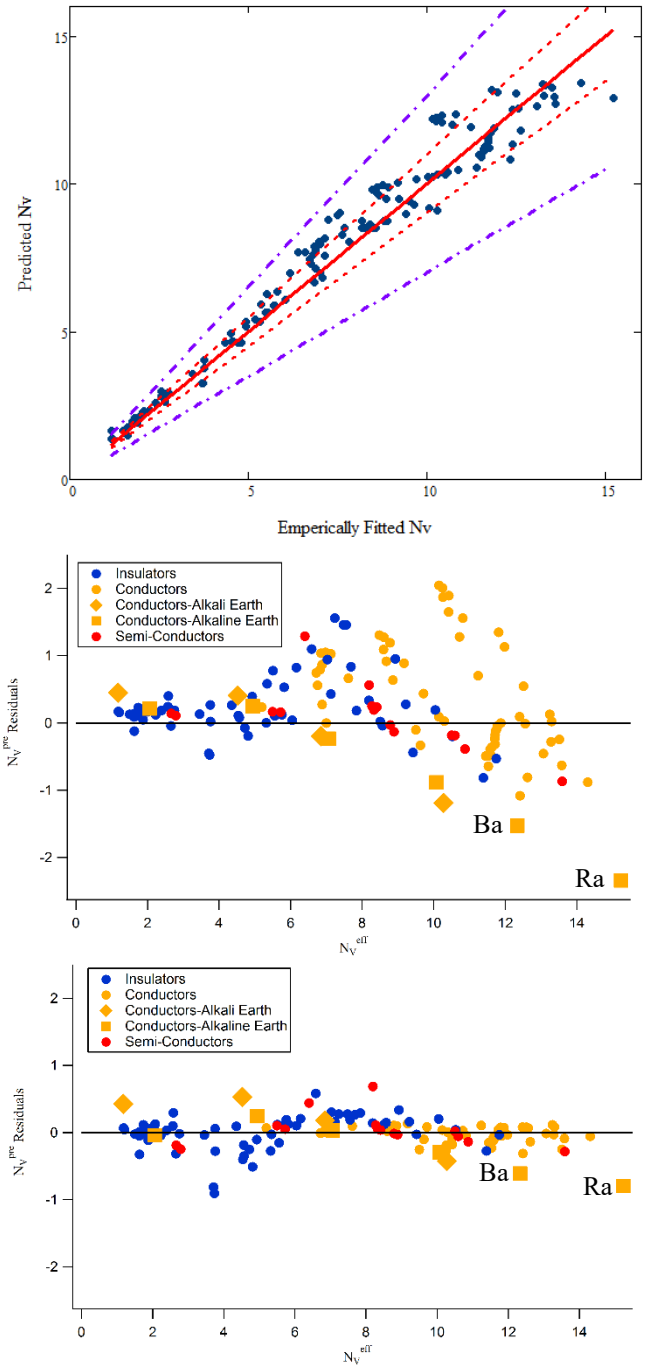


**Fig. 5. Comparison of predicted $N_V^{pre}$ values to empirical $N_V^{eff}$ values. (a) Predicted $N_V^{pre}$ values [using (5)] versus empirical $N_V^{eff}$ values. The red and purple dashed lines represent 10% and 30% deviations, respectively, from an exact one-to-one linear fit (solid red). (b) Residuals $(N_V^{pre} - N_V^{eff})$ [using (5)] versus empirical $N_V^{eff}$ values. (c) Residuals $(N_V^{pre} - N_V^{eff})$ values [using (7) with density correction] versus empirical $N_V^{eff}$ values.**

To assess the ability of (7) to accurately predict $N_V^{eff}$, Fig. 5(c) plots the residuals $(N_V^{pre} - N_V^{eff})$ [using (7)] against the empirical $N_V^{eff}$ values. It is evident that the density correction

**Table II. Fitting parameters and goodness of fit for predictive $N_V^{pre}$ model with density correction [Eq. (7)].**

| Materials | $N_o$ | $n_o$ | $N_{offset}$ | $N_1$ | $n_1$ | $\chi^2_{Nv}$ | $r_{Nv}$ |
|---|---|---|---|---|---|---|---|
| All | 6.91 | 0.240 | 1.067 | 0.202 | 0.144 | 1.492 | 0.988 |
| Insulators | 8.625 | 0.212 | 1.603 | 0.188 | 0.144 | 0.861 | 0.986 |
| Conductors | 7.361 | 0.236 | 1.114 | 0.207 | 0.144 | 0.251 | 0.948 |
| Semiconductors | 5.202 | 0.289 | 0.995 | 0.268 | 0.144 | 0.109 | 0.997 |

term reduced almost all deviations to below 10%, with a much improved correlation coefficient of $r = 0.988$.

### C. *Range Accuracy*

To further assess the validity of the predictive formula for $N_V^{pre}$ with density correction, (7), comparisons are made of ranges residuals calculated with both empirical $N_V^{eff}$ and predicted $N_V^{pre}$ (found in Table 2). Comparisons are shown in Figs. 4(b) and 4(c) for Au, Si, $SiO_2$, $Al_2O_3$, Al and Li. Fig. 4(b) shows the percent difference between the calculated range using $N_V^{pre}$ and (7) and the calculated range using $N_V^{eff}$ as a function of energy. Fig. 4(c) shows the percent difference between the calculated range using $N_V^{pre}$ and (7) and the range from the NIST ESTAR range and IMFP databases. The benefits of this correction for metals are clearly visible. The change in the $N_V^{pre}$ for conductors can reduce residuals from as high as 50% to <5% as seen for Au. Li, an alkali metal, is once again an outlier similar to the other alkali and alkaline metals as shown in Fig. 4(b) and 4(c). However, while Li has the greatest $\tilde{\chi}^2$=3·10$^{-5}$ [see Fig. 2(b)], it still exhibits good agreement with data and is nearly identical when using $N_V^{eff}$ versus $N_V^{pre}$. Non-metals and compounds do not see a large improvement from the density corrections, since the correction is based on metallic bonding between atoms; however, they also do not exhibit large changes in range residuals [see Fig. 4(c)] and $N_V^{pre}$ still remains within ~10% of $N_V^{eff}$ [see Fig. 5(c)].

## V. ESTIMATION OF ENERGY GAPS

In order to perform range calculations, a value for the electron band gap is needed for each material. However, the band gap is a more difficult parameter to determine than the stoichiometry or $\rho_m$; this is especially true for some insulators, liquids and gases, and compounds, polymers and composites. Band gaps for conductors and conductive alloys can be set to zero, with $\bar{E}$ determined by the effective plasmon energy, $E_p^{eff}$. Band gaps for many semiconductors and some insulators are readily available in [2] and [14]. Tabulated energy gaps for different crystalline forms of the wide bandgap semiconductors BN and AlN [14] have been used with (1) to estimate the effect of changes in density and bandgap on the range for these allotropes, as detailed in Section VII.

Fig. 6 shows the results of a study of the effect of changing the band gap on the predicted range. For a large bandgap insulator $Al_2O_3$ ($E_{gap}$=8.5 eV), even ±30% (±2.6 eV) variations in band gap energy change $N_V^{eff} \lesssim 10\%$ and $\tilde{\chi}^2 \lesssim 15\%$. Similar results for variations in band gap energies were found for many other materials [10].

Given the insensitivity to variations in band gap energies, other methods can be used to adequately estimate the appropriate energy gap for use with (3). Optical absorption and reflection spectroscopy, photoemission spectroscopy, and

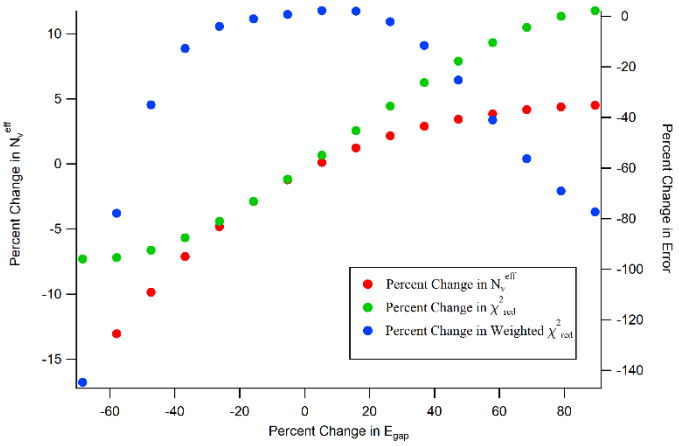


**Fig. 6. Effect of bandgap on the predicted range for alumina $SiO_2$. The fractional change in the band gap ($E_{gap}$=9.5 eV) versus the fractional change in $N_V^{eff}$ (●) and the fractional change in fitting error.**

thermal activation energies in electrical conductivity are common experimental methods to determine energy gaps [14]. For some materials with bandgaps in the visible range or lower, $E_{gap}$ might be estimated sufficiently well based solely of the color of the material.

As an example, optical absorption edges measured with VUV absorbance spectroscopy—which were correlated closely with the ionization energy in the study—were measured for a series of linear and cyclic alkane molecules [15]. These energy gaps were then used to calculate the range for these materials, most of which lacked data in the NIST databases. Work is in progress to compare range values calculated using optical absorption edge energies for these molecular materials to the tabulated NIST range values and thereby to assess the accuracy of using such surrogate energies.

For other materials—including gases, liquids, and highly disordered solids—for which band gap is not a well-defined concept, the highest occupied molecular orbital-to-lowest unoccupied molecular orbital (HOMO-LUMO) gap, $E_{HL}$, can provide a reasonable surrogate for the band gap in solids [16]. We propose a potential connection to the range through (3) for $E_m$ by adding $E_{HL}$ to the geometric mean of the effective plasmon energy and the bandgap energy as

$$E_m = 2.8\left[\left(E_p^{eff}\right)^2 + \left(E_{gap}\right)^2 + \left(E_{HL}\right)^2\right]^{1/2}. \quad (8)$$

There are many calculations of the $E_{HL}$ (often referred to as the Kohn-Sham band gap) in the literature, many of which are calculated using density function theory [16]. Alternately, $E_{HL}$ for reasonably complex molecular or polymeric materials and compounds can be calculated using available quantum chemistry computational packages such as Gaussian [17].

Estimates of the appropriate energy gaps for composite materials and complex biological materials listed in the NIST databases (*e.g.,* brain tissue and cortical bone tissue) are obviously much more difficult and ill-defined. For these

| Material | Formula | $\bar{Z}_A$ | $\rho_M$ $(g/cm^3)$ | $\bar{M}_A$ $(amu)$ | $N_V$ | $E_{gap}$ $E_{HL}$ $(eV)$ |
|---|---|---|---|---|---|---|
| PEEK | $C_{21}H_{18}O_3$ | 4.00 | 1.32 | 7.58 | 1.09 | 3.1 |
| PI (Kapton) | $C_{22}H_{10}N_2O_5$ | 5.01 | 1.42 | 9.77 | 1.51 | 2.32 |
| Deuterated PI | $C_{22}H_5D_5N_2O_5$ | 5.03 | 1.42 | 9.93 | 1.09 | 2.32 |
| PMMA (Lucite) | $C_6H_8O_2$ | 3.82 | 1.19 | 7.15 | 0.96 | 3.7 |
| Tin-Rich ITO | $(In_2O_3)_{0.904}(SnO_2)_{0.096}$ | 24.17 | 6.80 | 55.02 | 1.09 | 4.11 |
| Pentane | $C_5H_{12}$ | 2.47 | 0.63 | 4.24 | 0.33 | 7.18 |
| Hexane | $C_6H_{14}$ | 2.50 | 0.66 | 4.31 | 0.34 | 7.14 |
| Heptane | $C_7H_{16}$ | 2.52 | 0.68 | 4.36 | 0.36 | 7.09 |
| Octane | $C_8H_{18}$ | 2.54 | 0.70 | 4.40 | 0.36 | 7.06 |
| Decane | $C_{10}H_{22}$ | 2.56 | 0.73 | 4.45 | 0.38 | 7.05 |
| Boron Nitride (Cubic) | $BN$ | 6 | 3.45 | 12.41 | 1.64 | 6.2 |
| Boron Nitride (Hexagonal) | $BN$ | 6 | 2.1 | 12.41 | 1.80 | 5.2 |
| Boron Nitride (Wurtzite) | $BN$ | 6 | 3.49 | 12.41 | 1.64 | 5 |
| Boron Nitride (Amorphous) | $BN$ | 6 | 2.28 | 12.41 | 1.77 | 5.05 |
| Aluminum Nitride (Wurtzite) | $AlN$ | 10 | 3.26 | 20.50 | 2.78 | 6.02 |

**Table III. Material data for PEEK, normal and partially deuterated polyimide, PMMA, and tin-rich ITO where $E_{gap}$ is the band gap. The table also includes Pentane, Hexane, Heptane, Octane and Decane where $E_{HL}$, the HOMO/LUMO gap, is used. Different structures can lead to different densities as shown by the various forms of Boron Nitride. Aluminum Nitride is also included.**

materials, fits to NIST database values have been used to empirically determine $N_V^{eff}$, which in turn can lead to estimates of an effective energy gap.

## VI. Publically Available User Tool

An HTML/Javascript webpage has been developed to provide an easy to use tool for users to plot the 249 pre-defined materials. It also contains a tool to use the predictive method, so that the range can be estimated for arbitrary materials based solely on stoichiometry, mass density, and estimated band gap energy. The webpage also includes a download link for two *Excel* worksheets, one, the material database with material properties and the tool parameters, and second, a range approximation worksheet. Details can be found in [18].

## VII. Applications

Because new materials are developed faster than they can be characterized, it is important to have a quick predictive range formula. An example of a material with myriad spacecraft applications for which there are no published range data is polyether ether ketone (PEEK). Values of chemical formula, density, and band gap for PEEK [18,19] are listed in Table III, along with data for two similar polymers, polyimide and PMMA, for comparison. As shown in Fig. 7, the electron range for PEEK is predicted to be slightly greater than

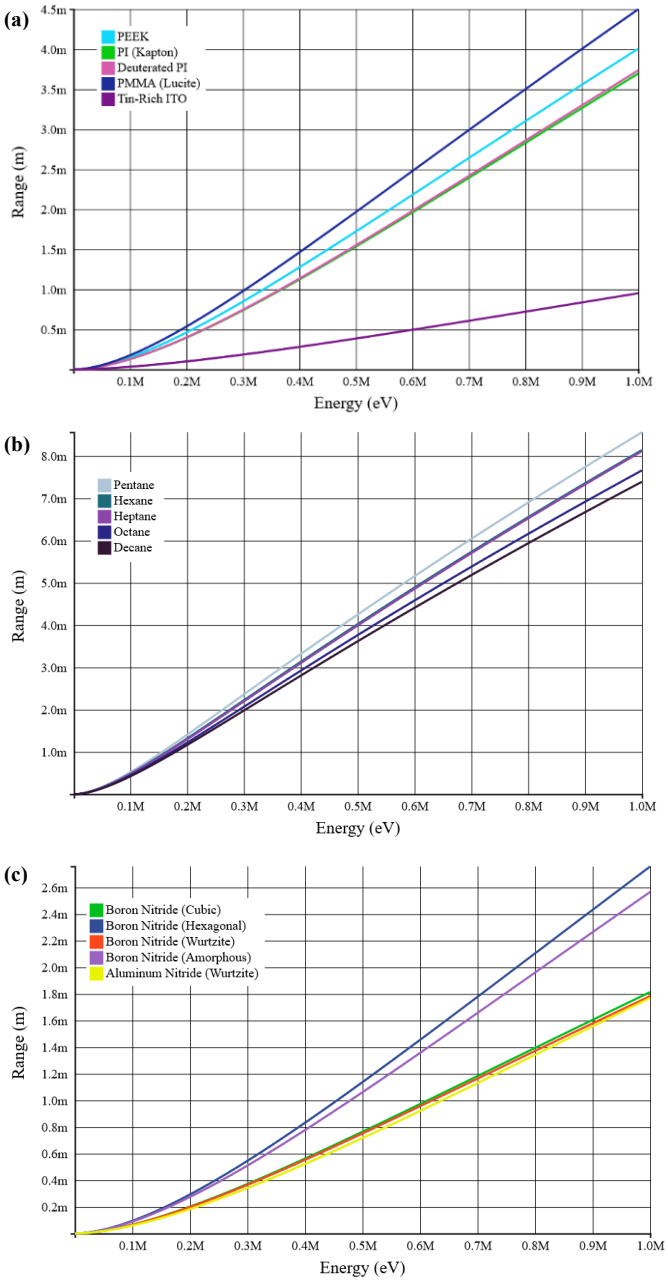


**Fig. 7. Electron range versus incident energy for (a) PEEK, polyimide, PMMA, and ITO (b) Pentane, Hexane, Heptane, Octane, and Decane (c) various forms of Boron Nitride and Aluminum Nitiride using a linear scale.**

polyimide and slightly less than PMMA. Similar data and calculations are also shown that contrast normal polyimide with polyimide with 50% deuterium. Fig. 7 shows the electron range for deuterated polyimide is predicted to be only slightly greater than normal polyimide.

An important example of range calculations for non-stochometric materials is indium-tin-oxide (ITO), a heavily doped n-type semiconductor which finds important uses as an optically transparent, electrically conducting ternary oxide alloy glass or ceramic. The optical band gap is largest at 4.20 eV for 5% $SnO_2$ by weight and reduces to 4.09 eV in the tin-rich (15% $SnO_2$ by weight) alloy [19]. Calculations are listed in Table III. Figure 7(a) shows that the electron range for tin-rich ITO is predicted to be less than normal polyimide.

Another useful example is the prediction of the range for a set of alkanes. Because the band gap is not applicable here, the HOMO/LUMO gap calculated using Gaussian is used instead. Calculations for the fitting parameters and required material properties are listed in Table III. Figure 7 (b) shows the electron range for pentane, hexane, heptane, octane, and decane.

Different structures can also effect the range. To show the changes in range, boron nitride is used as an example, investigating four different crystal structures with different bandgaps and densities. From the graph in Fig. 7(c), it shows that the range tends to increase slightly with decreasing density with very little change due to the changes in bandgap.

## VIII. CONCLUSION

Simulations were performed to test the sensitivity of $N_V^{eff}$ and the range to materials parameters; these suggest that reasonably accurate results were achievable with modest precision of the parameters. These correlations have led to methods using only basic material properties to predict $N_V^{eff}$ and thus the range for additional untested materials which have no supporting range data. These calculations are of great value for studies involving energetic electron bombardment, such as electron spectroscopy, spacecraft charging, or electron beam therapy. To make these range calculations easily accessible to the public, two user tools have been developed and can be accessed at the website in [18]

Future work related to this model will:

- Extend the database of materials with predicted $N_V^{pre}$ and range vesus energy data by considering tabulated energy gaps and other ways to estimate energy gaps for additional materials. Where possible, comparisons will be made of $N_V^{eff}$ and $N_V^{pre}$ and the predicted range data to range data from the NIST databases and similar sources.
- Evaluate the extention of the range model to better model liquids and gases by considering a possible surrogate of the band gap in solids for liquids and gases, using the highest occupied molecular orbital-to-lowest unoccupied molecular orbital (HOMO-LUMO) gap, $E_{LH}$ [17]. Where possible, comparisons will be made of $N_V^{eff}$ and $N_V^{pre}$ and the predicted range data to range data from the NIST databases and similar sources.
- Develop a better relativistic approximation to improve range predictions above $m_e c^2$=0.5 MeV, more closely based on the original range work of Bethe [21]. This should substaintially reduce the range versus energy residuals for the alkali and alkaline elemental metals and alkali halide compund materials, as exemplified by Li in Fig. 1.
- Model the approximate internal charge deposition profile as the fraction of electrons deposited as a function of penetration depth scaled by the range determined by the predictive formula for $N_V^{pre}$ through convolution of a universal normalized deposition curve [10].

These updates and changes as well as other future improvements will be applied to the online range tool in order to keep it up to date.

## ACKNOWLEDGEMENT

We gratefully acknowledge useful conversations with Robert Meloy from NASA Goddard Space Flight Center.

1. National Research Council. Committee on Nuclear Science, *Studies in Penetration of Charged Particles in Matter*. (National Academy of Sciences-National Research Council, 1964).
2. National Institute of Standards and Technology, 2010, "ESTAR, Stopping Power and Range Tables for Electrons," (http://physics.nist.gov/PhysRefData/Star/Text/ESTAR.html).
3. National Institute of Standards and Technology, 2010, "NIST Electron Inelastic-Mean-Free-Path Database: Version 1.1," (http://www.nist.gov/data/nist71.htm).
4. Wilson, G., and Dennison, J.R., 2010, "Approximation of range in materials as a function of incident electron energy," IEEE Trans. on Plasma Sci., **40**(2), 305-310.
5. Tanuma, A. S., Powell, C. J., and Penn, D.R., 1997, "Calculations of Electron Inelastic Mean Free Paths (IMFPs) VI. Analysis of the Gries Inelastic Scattering Model and Predictive IMFP Equation," Surf. Inter. Anal. 25, 25.
6. TN Rhodin and JW Gadzuk, "The Nature of the Surface Chemical Bond, ed. by TN Rhodin, G. Ertl", (North Holland, Amsterdam, 1979).
7. Gabor A Somorjai, Chemistry in two dimensions: surfaces. (Cornell University Press, 1981).
8. David R Penn, "Quantitative chemical analysis by ESCA," Journal of Electron Spectroscopy and Related Phenomena 9 (1), 29-40 (1976).
9. Wilson G. and Dennison, J.R., "Approximation of Range in Materials as a Function of Incident Electron Energy," *Proc. 11th Spacecraft Charging Tech. Conf.,* (Albuquerque, NM, September 20-24, 2010), 6 pp
10. Starley, A., Phillipps, L., Wilson, G., Dennison, J.R., 2015, "Predictive Formula for Electron Range over a Large Span of Energies," Am. Phys. Soc. Four Corners Meeting, Mesa, AZ.
11. Quist, T., Moore, B., Wilson, G., and Dennison, J.R., 2013, "Electron Penetration Ranges as a Function of Effective Number of Valence Electrons," Utah State University Student Showcase, Logan, UT.
12. Starley, A., Wilson, G., Phillipps, L.M. and Dennison, J.R., "Predictive Formula for Electron Penetration Depth of Diverse Materials over Large Energy Ranges," *Proc. of the* 14*th Spacecraft Charging Techn. Conf.,* (Space Research and Technology Centre of the European Space Agency (ESA/ESTEC), (Noordwijk, Netherlands, April 4-8, 2016).
13. Atkins, P.W., 1995, *The Periodic Kingdom*, Harper Collins, New York.
14. Strehlow, W. H. and Cook, E.L., 1973, "Compilation of Energy Band Gaps in Elemental and Binary Compound Semiconductors and Insulators," J. Phys. Chem. Ref. Data, 2(1), 163-199.
15. Costner, E.A., *et al*., 2009, "Fundamental Optical Properties of Linear and Cyclic Alkanes: VUV Absorbance and Index of Refraction," J. Phys. Chem. 113(33), 9337-9347.
16. Ueno, N., 2012, "Electronic Structure of Molecular Solids: Bridge to the Electrical Conduction," in *Physics of Organic Semiconductors*, Second Edition. Edited by W. Brutting and C. Adachi, Wiley-VCH Verlag, New York.
17. Frisch, M. J., *et al.*, 2004, *Gaussian 03*, Revision C.02, Gaussian, Inc., Wallingford CT, USA.
18. Wilson, G., Starley, A., and Dennison, J.R., "Electron Range Computational Tool for Arbitrary Materials over a Wide Energy Range," 15th Spacecraft Charging Technology Conference, Kobe University, (Kobe, Japan, June 25-29, 2018) (https://mpg.physics.usu.edu/range/).
19. Ho, J., Olguin, M., and Diaz, C. (2014). "Poly(Aryl -Ether -Ether-Ketone) as a Possible Metalized Film Capacitor Dielectric: Accurate Description of the Band Gap Through *Ab Initio* Calculation", Army Research Laboratory, TR-7160.
20. Kim, H., Gilmore, C. M. (1999). "Electrical, optical, and structural properties of indium-tin-oxide thin films for organic light-emitting devices", J Appl. Phys., 86(11), 6451-6461.
21. Bethe H., and Heitler, W., 1934, "On the Stopping of Fast Particles and on the Creation of Positive Electrons," in Proc. Royal Soc. London. Series A, Containing Papers of a Mathematical and Physical Character 146, 83.

**Greg Wilson** received dual B.S. degrees in physics and mathematics from Utah State University in Logan, UT in 2012. He received an MS in physics from Montana State University in Bozeman, MT in 2015. He is currently a PhD student in physics at Utah State University. He has worked with the Materials Physics Group for four years on electron emission and luminescence studies related to spacecraft charging. He is currently working for National Technical Systems as a Senior Engineer.

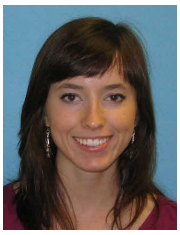

**Anne Starley** received B.S. degrees in physics from Utah State University in Logan, UT in 2012. She worked with the Materials Physics Group for 18 months on electron range modelling and pulsed electroacoustic studies related to spacecraft charging.

**Lisa Montierth Phillipps** received a BS in mechanical engineering in 2014 from Utah State University in Logan, UT. She previously worked in the Space Environment Effects Group at Space Dynamics Laboratory in Logan, UT in mechanical design and worked for two years with the Materials Physics Group on instrumentation design and electron range modelling.

**JR Dennison** received the B.S. degree in physics from Appalachian State University, Boone, NC, in 1980, and the M.S. and Ph.D. degrees in physics from Virginia Tech, Blacksburg, in 1983 and 1985, respectively. He was a Research Associate with the University of Missouri—Columbia before moving to Utah State University (USU), Logan, in 1988. He is currently a Professor of physics at USU, where he leads the Materials Physics Group. He has worked in the area of electron scattering for his entire career and has focused on the electron emission and conductivity of materials related to spacecraft charging for the last three decades. IEEE member since 2013.